A Single-Ended-to-Balanced Impedance-Transforming Branch-Line Coupler With Arbitrary Power Division Ratio

Lin Li, Jun-Fa Mao, *Fellow, IEEE*, and Lin-Sheng Wu, *Senior Member, IEEE*

***Abstract*— In this paper, a new single-ended-to-balanced (SETB) impedance-transforming branch-line coupler with the arbitrary power division ratio is presented. By using the matrix transformation, the standard scattering matrix and corresponding odd- and even-mode matrices are deduced from the mixed-mode scattering matrix. A simple configuration composed of four quarter-wavelength and two half-wavelength microstrip lines is proposed to achieve desired functions of the SETB branch-line coupler with the arbitrary power division ratio and arbitrary terminated impedances. The parameter selection and design principle are given. Finally, three prototypes with different power division ratios and terminated impedances are designed to verify the theoretical prediction. Impedance matching, port isolation, and mode conversion suppression are all obtained successfully for all the three fabricated SETB branch-line couplers. The proposed configuration also offers other attractive advantages including simpler configuration and design method, lower insertion loss, and good compatibility with the planar circuit technique.**

***Index Terms*— Branch-line coupler, impedance transforming, matrix transformation, power division, single-ended-to-balanced (SETB).**

I. Introduction

RECENTLY, a new direction of improvements has been introduced focusing on the development of the balanced circuit since they have high immunity to the environmental noise than their single-ended (SE) counterparts. There have been lots of efforts to make power dividers [1]–[5], filters [6]–[11], branch-line couplers [12], [13], and hybrid ring [14] fully balanced. SE-to-balanced (SETB) components are also getting lot of attention since both balanced and SE parts may be included in a circuit. In-phase and out-of-phase SETB power dividers have been proposed in [15]–[19]. SETB hybrid with the arbitrary power division ratio is presented in [20].

Manuscript received February 14, 2018; revised June 11, 2018; accepted July 8, 2018. Date of publication January 30, 2019; date of current version March 5, 2019. This work was supported in part by the National Natural Science Foundation of China under Grant 61361166010, Grant 51407156, Grant 61402417, and Grant 61234001 and in part by the Zhejiang Provincial Natural Science Foundation of China under Grant LY14E070009. *(Corresponding author: Lin-Sheng Wu.)*

L. Li is with the Key Laboratory of Ministry of Education for Design and Electromagnetic Compatibility of High-Speed Electronic Systems, Shanghai Jiao Tong University, Shanghai 200240, China, and also with the College of Information, Zhejiang Sci-Tech University, Hangzhou 310018, China.

J.-F. Mao and L.-S. Wu are with the Key Laboratory of Ministry of Education for Design and Electromagnetic Compatibility of High-Speed Electronic Systems, Shanghai Jiao Tong University, Shanghai 200240, China (e-mail: jfmao@sjtu.edu.cn; wallish@sjtu.edu.cn).

Digital Object Identifier 10.1109/TMTT.2019.2892433

As one of the most critical and fundamental building blocks in communication systems, the branch-line coupler with good directivity and inherent 90° phase difference can be widely used in microwave applications, such as power amplifiers [21], balanced mixers [22], and antenna arrays [23]. Branch-line couplers with the arbitrary power division ratio are very useful since they can provide more flexible for different applications. It have been shown that branch-line couplers may have the arbitrary power division by using shorted parallel coupled line sections [24], microstrip series stubs [25] four independent external impedance transformers [26], and coupled ring resonators [27]. SETB branch-line couplers are very useful in some applications too. They can be used to connect SE outputs to differential fed circular-polarized (CP) patch antennas by using their two balanced quadrature phase outputs. In comparison with the conventional CP patch antenna, the new CP patch antenna using SETB branch-line couplers has lower cross-polar radiation [28]–[30]. Besides, SETB branch-line couplers can also behave as balanced-to-SE (BTSE) branch-line couplers. They can be utilized to connect the balanced outputs to the SE CP patch antennas by using their two SE quadrature phase outputs. They may also be required in designing balanced mixers when the input ports of the mixers are balanced. In addition, arbitrary terminated real impedances will also be a quite important function for low loss and miniaturization without the extra impedance transformer. Consequently impedance-transforming SETB branch-line couplers are very desirable for the applications when the port matching is not limited to 50 Ω.

Generally, the diagram shown in Fig. 1(a) can be employed to construct an impedance-transforming SETB branch-line coupler. However, the use of baluns and impedance transformers leads to large design complexity and large in-band insertion loss. Therefore, it is valuable to develop an SETB branch-line coupler, with its diagram shown in Fig. 1(b). The circuit topology shown in Fig. 1(b) is symmetric with respect to the central line (s–s'). To our knowledge, no such SETB branch-line couplers have been reported.

In this paper, an SETB impedance-transforming branch-line coupler is proposed. First, the ideal mixed-mode scattering matrix of the proposed coupler is presented, and its corresponding odd- and even-mode three-port networks are derived. Then, a six-port circuit composed of ideal transmission lines is proposed to realize the odd- and even-mode three-port networks. The detailed design procedure is provided to

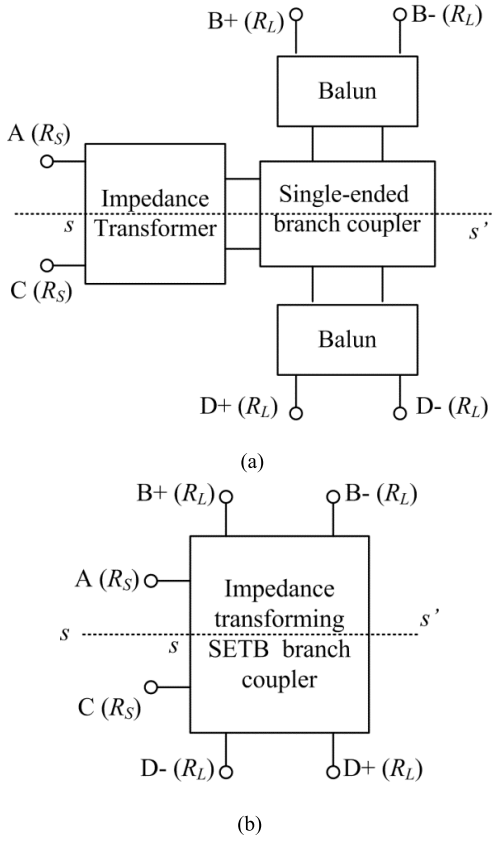

Fig. 1. Diagrams of impedance-transforming SETB branch-line coupler. (a) One SE branch-line coupler with two baluns and one impedance transformer. (b) Proposed diagram.

guide the practical design. Finally, three coupler prototypes with both tight and loose coupling power division ratios and different power division ratios, and terminated impedances are fabricated and measured to verify the theoretic prediction. The fabricated branch-line couplers show desired SETB power division characteristic with quadrature phase outputs, good impedance matching for both balanced and SE ports, high common-mode (CM) suppression for balanced ports, and high mode conversion suppression.

II. Theoretical Analysis

A. Mixed-Mode Scattering Matrix of Ideal Single-Ended-to-Balanced Branch-Line Coupler

The mixed-mode scattering matrix of the SETB branch coupler shown in Fig. 1(b) can be defined as [31]

$$[S^{mm}] = [M][S^{st}][M]^{-1} = \begin{pmatrix} S_{ssAA} & S_{sdAB} & S_{scAB} & S_{ssAC} & S_{sdAD} & S_{scAD} \\ S_{dsBA} & S_{ddBB} & S_{dcBB} & S_{dsBC} & S_{ddBD} & S_{dcBD} \\ S_{csBA} & S_{cdBB} & S_{ccBB} & S_{csBC} & S_{cdBD} & S_{ccBD} \\ S_{ssCA} & S_{sdCB} & S_{scCB} & S_{ssCC} & S_{sdCD} & S_{scCD} \\ S_{dsDA} & S_{ddDB} & S_{dcDB} & S_{dsDC} & S_{ddDD} & S_{dcDD} \\ S_{csDA} & S_{cdDB} & S_{ccDB} & S_{csDC} & S_{cdDD} & S_{ccDD} \end{pmatrix} \tag{1}$$

where the transformation matrix M can be described as

$$[M] = \frac{1}{\sqrt{2}} \begin{pmatrix} \sqrt{2} & 0 & 0 & 0 & 0 & 0 \\ 0 & 1 & -1 & 0 & 0 & 0 \\ 0 & 1 & 1 & 0 & 0 & 0 \\ 0 & 0 & 0 & \sqrt{2} & 0 & 0 \\ 0 & 0 & 0 & 0 & 1 & -1 \\ 0 & 0 & 0 & 0 & 1 & 1 \end{pmatrix}.$$

S_{dsBA}, S_{dsDA}, S_{dsBC}, and S_{dsDC} denote the SE-to-differential-mode (DM) transmission coefficients. S_{sdAB}, S_{sdAD}, S_{sdCB}, and S_{sdCD} denote the DM-to-SE transmission coefficients. S_{csBA}, S_{csDA}, S_{csBC}, and S_{csDC} denote the SE-to-CM transmission coefficients. S_{scAB}, S_{scAD}, S_{scCB}, and S_{scCD} denote the CM-to-SE transmission coefficients. S_{ssAA}, S_{ssCC}, S_{ssAC}, and S_{ssCA} are the SE S-parameters of the two SE ports. S_{ddBB}, S_{ddDD}, S_{ddBD}, and S_{ddDB} are the DM S-parameters of the two balanced ports. S_{ccBB}, S_{ccDD}, S_{ccBD}, and S_{ccDB} are the CM S-parameters of the two balanced ports. S_{cdBB}, S_{cdDD}, S_{cdBD}, and S_{cdDB} are the DM-to-CM conversion coefficients. S_{dcBB}, S_{dcDD}, S_{dcBD}, and S_{dcDB} are the CM-to-DM conversion coefficients.

Since the circuit topology shown in Fig. 1(b) is symmetric with respect to the central line (s–s'), the power division ratio between the two balanced output ports B and D is defined as

$$k = \left|\frac{S_{sdAB}}{S_{sdAD}}\right|^2 = \left|\frac{S_{sdCD}}{S_{sdCB}}\right|^2. \tag{2}$$

Let $x = \sqrt{k}j/\sqrt{1+k}$ and $y = -1/\sqrt{1+k}$, then

$$S_{sdAB} = S_{sdCD} = S_{dsBA} = S_{dsDC} = x \tag{3}$$

$$S_{sdAD} = S_{sdCB} = S_{dsDA} = S_{dsBC} = y. \tag{4}$$

Furthermore, the proposed SETB branch-line coupler should satisfy the impedance matching at the two SE ports A and C, DM impedance matching at the two balanced ports B and D, ports isolation between the two SE ports of A and C, and balanced ports' isolation between the two balanced ports of B and D. Consequently, the following equations should be satisfied:

$$S_{ssAA} = S_{ssCC} = 0 \tag{5}$$

$$S_{ddBB} = S_{ddDD} = 0 \tag{6}$$

$$S_{ssAC} = S_{ssCA} = 0 \tag{7}$$

$$S_{ddBD} = S_{ddDB} = 0. \tag{8}$$

For the CM operation, the CM signal should be reflected at both the two balanced ports. The CM transmission between the two balanced ports, the conversions between CM signal and DM signal, and the conversions between CM signal and SE signal should be suppressed. Therefore, the following equations can be obtained:

$$S_{ccBB} = S_{ccDD} = -1 \tag{9}$$

$$S_{ccBD} = S_{ccDB} = 0 \tag{10}$$

$$S_{cdBB} = S_{dcBB} = S_{cdDD} = S_{dcDD} = 0 \tag{11}$$

$$S_{cdBD} = S_{dcDB} = S_{cdDB} = S_{dcBD} = 0 \tag{12}$$

$$S_{csBA} = S_{csBC} = S_{csDA} = S_{csDC} = 0 \tag{13}$$

$$S_{scAB} = S_{scAD} = S_{scCB} = S_{scCD} = 0. \tag{14}$$

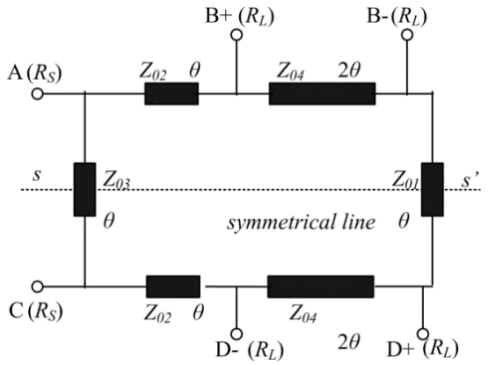

Fig. 2. Circuit model of the proposed branch-line coupler ($\theta = 90°$ at the center frequency f_0).

According to the relations between the mixed-mode scattering matrix $[S^{mm}]$ and the standard scattering matrix $[S^{st}]$, $[S^{st}]$ can be obtained from the following equation [31]:

$$[S^{st}] = [M]^{-1}[S^{mm}][M] \tag{15}$$

$$= \begin{pmatrix} [S_U] & [S_D] \\ [S_D] & [S_U] \end{pmatrix} \times \frac{1}{2\sqrt{2}} \begin{pmatrix} 0 & 2x & -2x & 0 & 2y & -2y \\ 2x & -\sqrt{2} & -\sqrt{2} & 2y & 0 & 0 \\ -2x & -\sqrt{2} & -\sqrt{2} & -2y & 0 & 0 \\ 0 & 2y & -2y & 0 & 2x & -2x \\ 2y & 0 & 0 & 2x & -\sqrt{2} & -\sqrt{2} \\ -2y & 0 & 0 & -2x & -\sqrt{2} & -\sqrt{2} \end{pmatrix} \tag{16}$$

where $[S_U]$ and $[S_D]$ are both 3×3 submatrices.

Therefore, the odd-mode and even-mode matrices can be obtained using the transformation technique given in [9]

$$[S_e] = [S_U] + [S_D] = \frac{1}{2\sqrt{2}} \begin{pmatrix} 0 & 2x+2y & -2x-2y \\ 2x+2y & -\sqrt{2} & -\sqrt{2} \\ -2x-2y & -\sqrt{2} & -\sqrt{2} \end{pmatrix} \tag{17}$$

$$[S_o] = [S_U] - [S_D] = \frac{1}{2\sqrt{2}} \begin{pmatrix} 0 & 2x-2y & -2x+2y \\ 2x-2y & -\sqrt{2} & -\sqrt{2} \\ -2x+2y & -\sqrt{2} & -\sqrt{2} \end{pmatrix}. \tag{18}$$

Based on the above derivation, the even-mode and odd-mode scattering matrices of the SETB branch coupler should have the forms of (17) and (17), respectively.

B. Realization of the SETB Branch-Line Coupler

In order to realize an SETB impedance-transforming branch coupler, the circuit shown in Fig. 2 is utilized. It consists of two quarter-wavelength transmission lines with characteristics impedance Z_{02}, two half-wavelength transmission lines with characteristics impedance Z_{04}, one quarter-wavelength transmission line with characteristics impedance Z_{01}, and one quarter-wavelength transmission line with characteristics impedance of Z_{03}.

Since the circuit shown in Fig. 2 is symmetric with respect to the central line (s–s'), the odd-mode and even-mode circuits

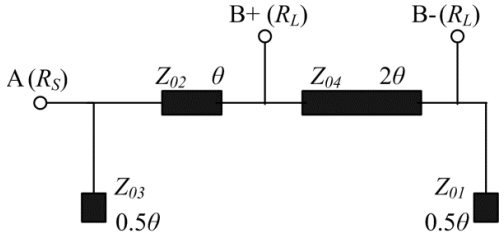

Fig. 3. Even-mode equivalent circuit of the proposed branch-line coupler.

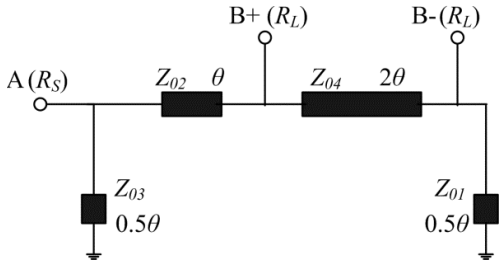

Fig. 4. Odd-mode equivalent circuit of the proposed branch-line coupler.

can be obtained by placing an electric wall and a magnetic wall along the symmetrical line, respectively. The even-mode and odd-mode equivalent circuits of the proposed SETB branch-line coupler are shown in Figs. 3 and 4, respectively.

As seen in Fig. 3, when port B− is terminated by R_L, we can calculate the two-port even-mode $ABCD$ matrix between ports A and B+ as follows:

$$\begin{pmatrix} A_e^{AB+} & B_e^{AB+} \\ C_e^{AB+} & D_e^{AB+} \end{pmatrix} = \begin{pmatrix} jZ_{02}\left(\frac{1}{R_L} + \frac{j}{Z_{01}}\right) & jZ_{02} \\ jY_{02} - Z_{02}Y_{03}\left(\frac{1}{R_L} + \frac{j}{Z_{01}}\right) & -Z_{02}Y_{03} \end{pmatrix}. \tag{19}$$

Then, the normalized $ABCD$ matrix is obtained as

$$\begin{pmatrix} a_e^{AB+} & b_e^{AB+} \\ c_e^{AB+} & d_e^{AB+} \end{pmatrix} = \begin{pmatrix} \frac{\sqrt{R_L}}{\sqrt{R_S}} A_e^{AB+} & \frac{1}{\sqrt{R_L R_S}} B_e^{AB+} \\ \sqrt{R_L R_S} C_e^{AB+} & \frac{\sqrt{R_S}}{\sqrt{R_L}} D_e^{AB+} \end{pmatrix}. \tag{20}$$

Considering the relationship between S-matrix and $ABCD$ matrix [32], we can get the two-port even-mode S-matrix between ports A and B+ from (19) using the following relations:

$$S_{AB+e} = S_{B+Ae} = \frac{2}{a_e^{AB+} + b_e^{AB+} + c_e^{AB+} + d_e^{AB+}} \tag{21}$$

$$S_{AAe} = \frac{a_e^{AB+} + b_e^{AB+} - c_e^{AB+} - d_e^{AB+}}{a_e^{AB+} + b_e^{AB+} + b_e^{AB+} + d_e^{AB+}} \tag{22}$$

$$S_{B+B+e} = \frac{-a_e^{AB+} + b_e^{AB+} - c_e^{AB+} + d_e^{AB+}}{a_e^{AB+} + b_e^{AB+} + c_e^{AB+} + d_e^{AB+}}. \tag{23}$$

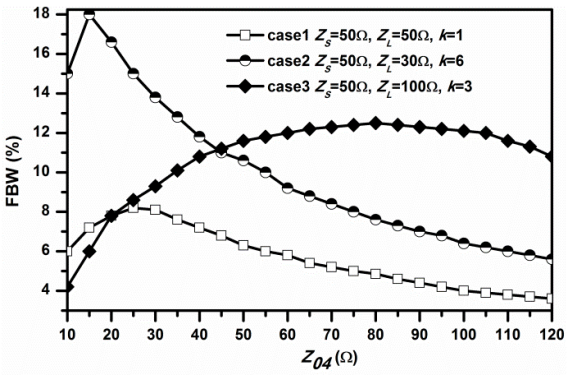

Fig. 5. FBW of the SETB branch-line coupler with variable Z_{04}.

Substituting the even-mode S-parameters in (17) into (21), (22), and (22), we can get the following equations:

$$\sqrt{R_L/R_S}Z_{02} - \sqrt{2}Z_{01}/\sqrt{1+k} = 0 \tag{24}$$

$$Z_{03} = 2Z_{01}R_S/R_L \tag{25}$$

$$Z_{02}^2(R_L R_S + 2Z_{01}Z_{03}) = R_L R_S Z_{01} Z_{03}. \tag{26}$$

From the above relations, we can get the solutions as

$$Z_{01} = \frac{\sqrt{k}R_L}{2} \tag{27}$$

$$Z_{02} = \frac{\sqrt{k}}{\sqrt{2(1+k)}}\sqrt{R_S R_L} \tag{28}$$

$$Z_{03} = \sqrt{k}R_S. \tag{29}$$

It can be easily verified that the proposed circuit shown in Fig. 2 has the same odd-mode and even-mode matrices as (17) and (17) once the equations of (27), (28), and (28) are satisfied.

Based on the above analyses, the impedance of Z_{01}, Z_{03}, and Z_{02} can be calculated from the predetermined power division ratio k and terminated impedances. When all terminated ports have the same 50-Ω impedance, the maximum power division ratio k is 6.25 if the realizable characteristic impedance of transmission line is within 16–125 Ω.

It can be observed that the characteristic impedance Z_{04} is a free variable in these analytical design equations and it exerts no influence on the responses at the center frequency (f_0). However, the influence of Z_{04} on the fractional bandwidth (FBW) should be studied. In order to determine the influence of Z_{04} on performance of the SETB branch-line coupler, three curves are plotted in Fig. 5 for four different cases. In the graph, FBW is defined by $|S_{ssAA}|$, $|S_{ssCC}|$, $|S_{ddBB}|$, $|S_{ddDD}|$, $|S_{ssAC}|$, and $|S_{ddDB}|$ under −15 dB. It is quite clear that FBW of the proposed SETB branch-line coupler can be adjusted by changing the value of Z_{04}. Maximum FBW can be obtained by selecting a proper Z_{04}.

The design guideline for this proposed SETB branch-line coupler can be briefly summarized as follows.

1) Specify the desired power-dividing ratio k and terminated impedances R_S and R_L.
2) Get the values of Z_{01}, Z_{02}, and Z_{03} according to (27)–(28).
3) Select the proper $Z_{04}$to obtain the bandwidth performance.
4) Choose the appropriate dimensions of the microstrip lines on predetermined substrate.
5) Optimize a bit if necessary.

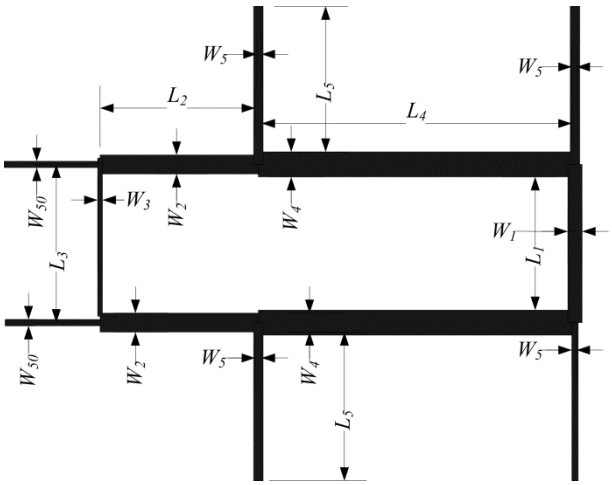

Fig. 6. Layout of the proposed SETB branch coupler.

TABLE I
THEORETICAL PARAMETERS OF THE THREE PROTOTYPES

	R_S (Ω)	R_L (Ω)	Z_{01} (Ω)	Z_{02} (Ω)	Z_{03} (Ω)	Z_{04} (Ω)
Design I (k=1)	50	50	25	25	50	25
Design II (k=3)	50	100	86.6	43.3	86.6	80
Design III (k=6)	50	30	36.75	25.35	122.5	15

III. EXPERIMENTAL VERIFICATION

For theoretical and experimental verification, three prototypes of the proposed SETB branch-line couplers centered at 2.5 GHz are designed, measured, and compared. For Design I with $k = 1$, the source impedance$R_s = 50\ \Omega$ and load impedance $R_L = 50\ \Omega$. For Design II with $k = 3$, the source impedance $R_s = 50\ \Omega$ and load impedance $R_L = 100\ \Omega$. For Design III with $k = 6$, the source impedance $R_s = 50\ \Omega$ and load impedance $R_L = 30\ \Omega$. All the three circuits are fabricated on 0.5-mm-thick substrate with the relative dielectric constant of 2.65 and loss tangent of 0.0035. In order to measure the circuit using the vector network analyzer directly, four quarter-wavelength lines with width W_5 and length L_5 are added between the input ports and the SETB branch-line coupler. Fig. 6 exhibits the layout of the proposed SETB branch-line couple with adding transmission-line impedance transformers.

According to the design procedure in Section II, the values of Z_{01}, Z_{02}, and Z_{03} for the three prototypes can be calculated by (27)–(28) and are listed in Table I. For obtaining the widest operating bandwidth, the value of Z_{04} is chosen from the curves shown in Fig. 5. The values of Z_{04} for the three prototypes are listed in Table I too.

According to the theoretical parameters shown in Table I, the final dimensions of the two prototypes are listed in Table II. The core circuit size of Design I, Design II, and Design III are 63.2 mm × 24.5 mm ($0.775\lambda_g \times 0.3\lambda_g$), 61.2 mm × 24.8 mm

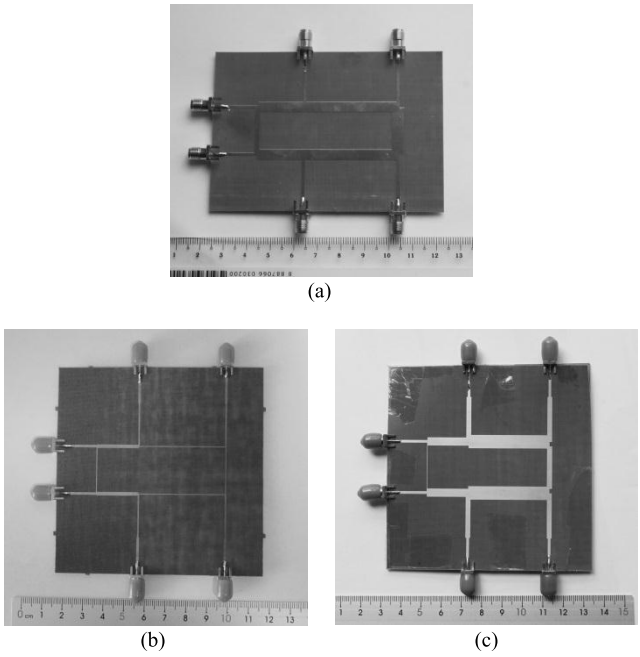

Fig. 7. Photograph of the fabricated coupler. (a) Design I. (b) Design II.

($0.75\lambda_g \times 0.3\lambda_g$), and 63.2 mm × 31.62 mm ($0.775\lambda_g \times 0.39\lambda_g$), where λ_g is the guided wavelength at f_0. Fig. 7 shows the three photographs of the proposed three designs.

The full-wave simulation of the designs was done by high frequency structure simulation. The measurement was done by a four-port vector network analyzer Agilent E5071. During measurement, the four-port S-parameters among any four ports can be obtained by connecting two 50-Ω standard loads to the other two ports. Then, the mixed-mode S-parameters are extracted from the standard S-parameters by using the relations between $[S^{mm}]$ and $[S^{st}]$.

Fig. 8(a)–(d) shows the simulated and measured results of Design I. As shown in Fig. 8, the SE matching bandwidth ($|S_{ssAA}| < -15$ dB) and DM matching bandwidth ($|S_{ddBB}| < -15$ dB) are 10.8% and 10% at the center frequency of 2.5 GHz. The SE mode isolation bandwidth of $|S_{ssAC}| < -15$ dB, the DM isolation bandwidth of $|S_{ddBD}| < -15$ dB, and the CM rejection bandwidth of $|S_{ccBD}| < -15$ dB are 10.5%, 9.8%, and 94.5%. The CM-to-SE mode suppression bandwidth ($|S_{scAB}|$ and $|S_{scAD}| < -20$ dB) is 12.8%, and the CM-to-DM suppression bandwidth ($|S_{dcBB}|$ and $|S_{dcBD}| < -20$ dB) is 14%. Impedance matching, port isolation, and mode conversion suppression are also obtained well for Design II. The measured phase difference between ports B and D is between 87.5° and 92.5° over the frequency range from 2.43 to 2.57 GHz, with 5.6% FBW. The measured $|S_{sdCB}|$ and $|S_{sdAB}|$ shown in Fig. 8 are −3.14 and −3.25 dB at 2.5 GHz, and the power division ratio at the center frequency is 0.975, which is close to the desired one.

Fig. 9(a)–(d) shows the simulated and measured results of Design II. As shown in Fig. 9, the SE matching bandwidth ($|S_{ssAA}| < -15$ dB) and DM matching bandwidth ($|S_{ddBB}| < -15$ dB) are 28% and 12% at the center frequency of 2.5 GHz. The SE mode isolation bandwidth of $|S_{ssAC}| < -15$ dB, the DM isolation bandwidth of $|S_{ddBD}| <$

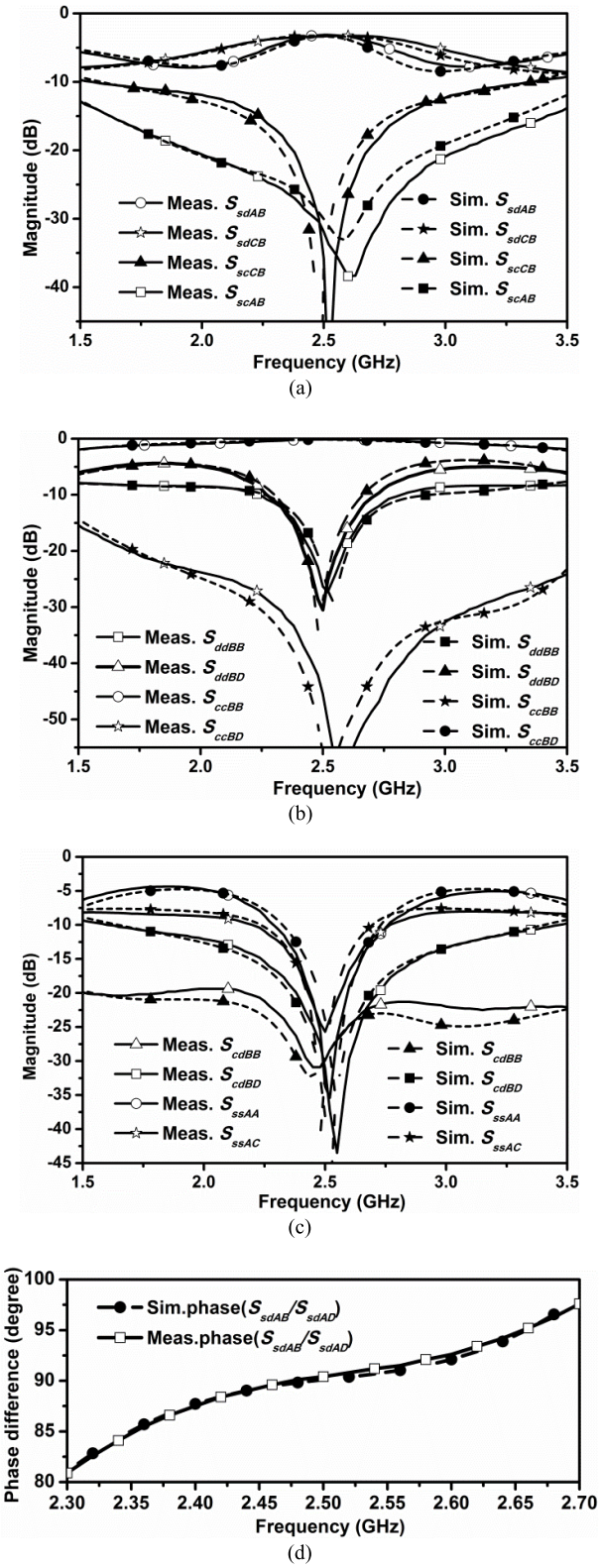

Fig. 8. Simulated and measured mixed-mode parameters of Design I. (a) $|S_{sd}|$ and $|S_{sc}|$. (b) $|S_{dd}|$ and $|S_{cc}|$. (c) $|S_{ss}|$ and $|S_{dc}|$. (d) Phase (S_{sdAB}/S_{sdAD}).

−15 dB, and the CM rejection bandwidth of $|S_{ccBD}| <$ −15 dB are 10.5%, 16.4%, and 55.2%. The CM-to-SE mode suppression bandwidth ($|S_{scAB}|$ and $|S_{scAD}| < -20$ dB) is 12%, and the CM-to-DM suppression bandwidth ($|S_{dcBB}|$

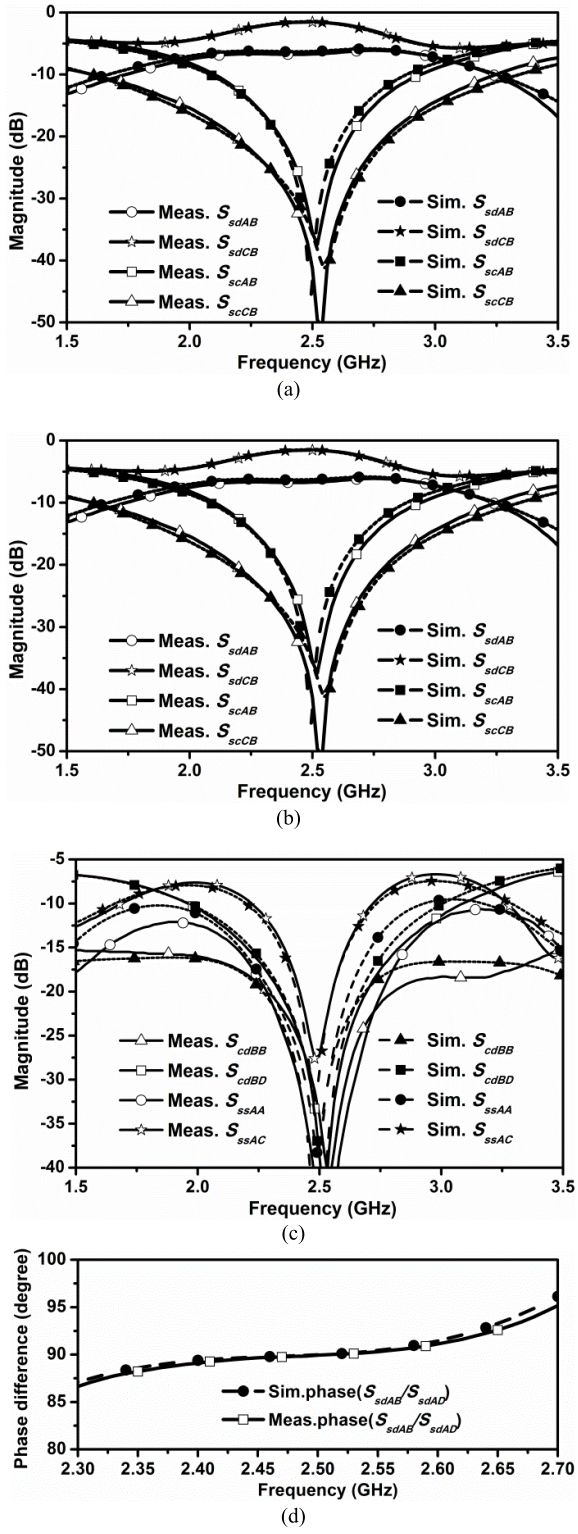

Fig. 9. Simulated and measured mixed-mode parameters of Design II. (a) $|S_{sd}|$ and $|S_{sc}|$. (b) $|S_{dd}|$ and $|S_{cc}|$. (c) $|S_{ss}|$ and $|S_{dc}|$. (d) Phase (S_{sdAB}/S_{sdAD}).

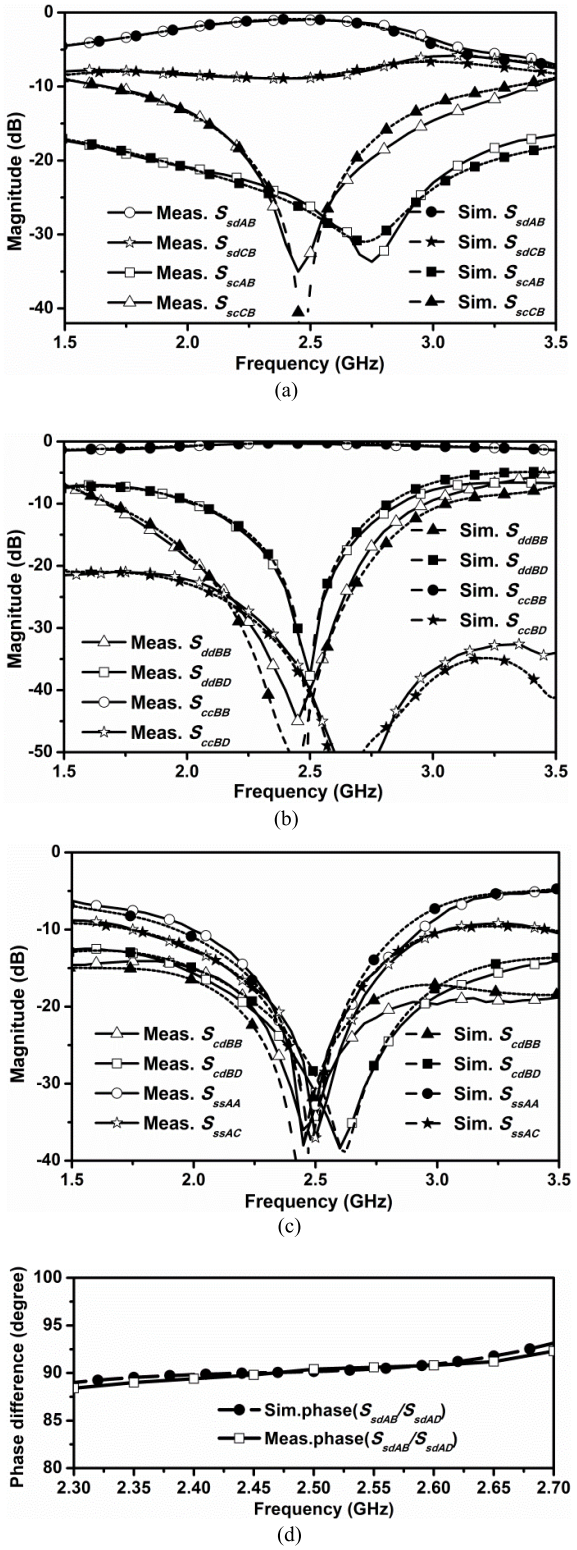

Fig. 10. Simulated and measured mixed-mode parameters of Design III. (a) $|S_{sd}|$ and $|S_{sc}|$. (b) $|S_{dd}|$ and $|S_{cc}|$. (c) $|S_{ss}|$ and $|S_{dc}|$. (d) Phase (S_{sdAB}/S_{sdAD}).

and $|S_{dcBD}| < -20$ dB) is 15.2%. Impedance matching, port isolation, and mode conversion suppression are also obtained well for Design II. The measured phase difference between ports B and D is between 87.5° and 92.5° over the frequency range from 2.32 to 2.65 GHz, with 13.2% FBW. The measured $|S_{sdCB}|$ and $|S_{sdAB}|$ shown in Fig. 9 are -1.57 and -6.5 dB at 2.5 GHz, and the power division ratio at the center frequency is 3.11, which is also close to the desired one.

Fig. 10(a)–(d) shows the simulated and measured results of Design II. As shown in Fig. 9, the SE matching bandwidth ($|S_{ssAA}| < -15$ dB) and DM matching bandwidth

TABLE II
DIMENSIONS OF THE THREE PROTOTYPES

	W_1 (mm)	L_1 (mm)	W_2 (mm)	L_2 (mm)	W_3 (mm)	L_3 (mm)	W_4 (mm)	L_4 (mm)	W_5 (mm)	L_5 (mm)	W_{50} (mm)
Design I	3.6	17.3	3.6	19.55	1.3	19.6	3.6	39.84	1.32	0	1.32
Design II	0.48	22.45	1.72	20.5	0.48	21.7	0.55	41.225	0.775	20	1.32
Design II	2.47	18.65	13.95	19.14	0.17	23.85	6.5	37.36	2.32	18.7	1.32

TABLE III
PERFORMANCE COMPARISON OF PREVIOUS WORKS AND THIS WORK

Ref.	Size (λ_g^2)	k	IL (dB)	Type	CMS	IT
[24]	N.A.	2,5	N.A.	SETSE	No	No
[25]	0.74×0.28	1.59	0.2	SETSE	No	No
[26]	0.55×0.55	3.16	0.8	SETSE	No	Yes
[13] Design I	0.52×0.5	1	0.45	BTB	Yes	No
[13] Design II	0.52×0.5	2	0.25	BTB	Yes	No
[13] Design III	0.52×0.5	4	0.1	BTB	Yes	No
[14]	0.42×0.33	1	1.4	BTB	Yes	No
Design I	0.78×0.3	1	0.25	SETB	Yes	Yes
Design II	0.75×0.3	3	0.48	SETB	Yes	Yes
Design III	0.78×0.4	6	0.5	SETB	Yes	Yes

SETSE, single-ended-to-single-ended; CMS, common-mode suppression; BTB, balanced-to-balanced; IL, insertion loss, IT, impedance transformation.

($|S_{ddBB}| < -15$ dB) are 24% and 38% at the center frequency of 2.5 GHz. The SE mode isolation bandwidth of $|S_{ssAC}| < -15$ dB, the DM isolation bandwidth of $|S_{ddBD}| < -15$ dB, and the CM rejection bandwidth of $|S_{ccBD}| < -15$ dB are 26.4%, 42%, and 108%. The CM-to-SE mode suppression bandwidth ($|S_{scAB}|$ and $|S_{scAD}| < -20$ dB) is 20%, and the CM-to-DM suppression bandwidth ($|S_{dcBB}|$ and $|S_{dcBD}| < -20$ dB) is 24.8%. Impedance matching, port isolation, and mode conversion suppression are also obtained well for Design III. The measured phase difference between ports B and D is between 87.5° and 92.5° over the frequency range from 2.28 to 2.72 GHz, with 17.6% FBW. The measured $|S_{sdCB}|$ and $|S_{sdAB}|$ shown in Fig. 10 are -0.95 and -8.8 dB at 2.5 GHz, and the power division ratio at the center frequency is 6.1, which is close to the desired one too.

The performances of the proposed designs and previous designs with the arbitrary power division are listed in Table III. Compared with the reported design, only the proposed one can be utilized in the SETB design. Besides, compared with the reported BTB design, the proposed one incorporates the function of the impedance transformation.

IV. CONCLUSION

In this paper, a new SETB impedance-transforming branch-line coupler is proposed. The coupler can remove the extra baluns and impedance transformers in the common coupler and make the circuit connect with balanced and SE circuits at the same time. The theoretical analysis and parameter design have been given, and the design procedure is summarized. Using the derived design equations, three prototypes are designed and fabricated. The measured results for the prototype agree well with the simulation results. The fabricated branch-line coupler shows the desired SETB power division characteristic with the merits of lower insertion loss, compact size, and simpler design method. The proposed SETB branch-line coupler can also behave a BTSE branch-line coupler.

REFERENCES

[1] L.-S. Wu, B. Xia, J.-F. Mao, and W.-Y. Yin, "A half-mode substrate integrated waveguide ring for two-way power division of balanced circuit," *IEEE Microw. Wireless Compon. Lett.*, vol. 22, no. 7, pp. 333–335, Jul. 2012.

[2] B. Xia, L.-S. Wu, and J.-F. Mao, "A new balanced-to-balanced power divider/combiner," *IEEE Trans. Microw. Theory Techn.*, vol. 60, no. 9, pp. 2791–2798, Sep. 2012.

[3] B. Xia, L.-S. Wu, S.-W. Ren, and J.-F. Mao, "A balanced-to-balanced power divider with arbitrary power division," *IEEE Trans. Microw. Theory Techn.*, vol. 61, no. 8, pp. 2831–2840, Aug. 2013.

[4] W. Feng, C. Zhao, W. Che, and Q. Xue, "A balanced-to-balanced network with unequal power division and wideband common mode suppression," *IEEE Microw. Wireless Compon. Lett.*, vol. 26, no. 4, pp. 237–239, Apr. 2016.

[5] J. Shi, J. Wang, K. Xu, J.-X. Chen, and W. Liu, "A balanced-to-balanced power divider with wide bandwidth," *IEEE Microw. Wireless Compon. Lett.*, vol. 25, no. 9, pp. 573–575, Sep. 2015.

[6] C.-H. Wu, C.-H. Wang, and C.-H. Chen, "Novel balanced coupled-line bandpass filters with common-mode noise suppression," *IEEE Trans. Microw. Theory Techn.*, vol. 55, no. 2, pp. 287–295, Feb. 2007.

[7] T. B. Lim and L. Zhu, "A differential-mode wideband bandpass filter on microstrip line for UWB application," *IEEE Microw. Wireless Compon. Lett.*, vol. 19, no. 10, pp. 632–634, Oct. 2009.

[8] L. Li, J. Bao, J.-J. Du, and Y.-M. Wang, "Differential wideband bandpass filters with enhanced common-mode suppression using internal coupling technique," *IEEE Microw. Wireless Compon. Lett.*, vol. 24, no. 5, pp. 300–302, May 2014.

[9] H. Wang, L.-M. Gao, K.-W. Tam, W. Kang, and W. Wu, "A wideband differential BPF with multiple differential- and common-mode transmission zeros using cross-shaped resonator," *IEEE Microw. Wireless Compon. Lett.*, vol. 24, no. 12, pp. 854–856, Dec. 2014.

[10] W. Feng and W. Che, "Novel wideband differential bandpass filters based on T-shaped structure," *IEEE Trans. Microw. Theory Techn.*, vol. 60, no. 6, pp. 1560–1568, Jun. 2012.

[11] X. Guo, L. Zhu, K.-W. Tam, and W. Wu, "Wideband differential bandpass filters on multimode slotline resonator with intrinsic common-mode rejection," *IEEE Trans. Microw. Theory Techn.*, vol. 63, no. 5, pp. 1587–1594, May 2015.

[12] J. Shi *et al.*, "A balanced filtering branch-line coupler," *IEEE Microw. Wireless Compon. Lett.*, vol. 26, no. 2, pp. 119–121, Feb. 2016.

[13] J. Shi, J. Qiang, K. Xu, and J.-X. Chen, "A balanced branch-line coupler with arbitrary power division ratio," *IEEE Trans. Microw. Theory Techn.*, vol. 65, no. 1, pp. 78–85, Jan. 2017.

[14] K. Xu, J. Shi, J. Lu, W. Zhang, and J.-X. Chen, "Balanced ring hybrid with arbitrary power division ratio," *Electron. Lett.*, vol. 53, no. 11, pp. 726–728, May 2017.

[15] W. Zhang, Y. Wu, Y. Liu, F. M. Ghannouchi, and A. Hasan, "A wideband balanced-to-unbalanced coupled-line power divider," *IEEE Microw. Wireless Compon. Lett.*, vol. 26, no. 6, pp. 410–412, Jun. 2016.

[16] J. Shi, J. Lu, K. Xu, and J.-X. Chen, "A coupled-line balanced-to-single-ended out-of-phase power divider with enhanced bandwidth," *IEEE Trans. Microw. Theory Techn.*, vol. 65, no. 2, pp. 459–466, Feb. 2017.

[17] A. N. Yadav and R. Bhattacharjee, "Balanced to unbalanced power divider with arbitrary power ratio," *IEEE Microw. Wireless Compon. Lett.*, vol. 26, no. 11, pp. 885–887, Nov. 2016.

[18] X. Gao, W. Feng, W. Che, and Q. Xue, "Wideband balanced-to-unbalanced filtering power dividers based on coupled lines," *IEEE Trans. Microw. Theory Techn.*, vol. 65, no. 1, pp. 86–95, Jan. 2017.

[19] K. Xu, J. Shi, L. Lin, and J.-X. Chen, "A balanced-to-unbalanced microstrip power divider with filtering function," *IEEE Trans. Microw. Theory Techn.*, vol. 63, no. 8, pp. 2561–2569, Aug. 2015.

[20] L. Li, L. S. Wu, and J.-F. Mao, "A balanced-to-unbalanced hybrid ring with arbitrary power division ratio," *IEEE Access*, vol. 6, pp. 19784–19790, 2018.

[21] W. Chen *et al.*, "Design and linearization of concurrent dual-band Doherty power amplifier with frequency-dependent power ranges," *IEEE Trans. Microw. Theory Techn.*, vol. 59, no. 10, pp. 2537–2546, Oct. 2011.
[22] S.-J. Lee, T.-J. Baek, M. Han, S.-G. Choi, D.-S. Ko, and J.-K. Rhee, "94 GHz MMIC single balanced mixer for FMCW radar sensor application," in *Proc. 5th Global Symp. Millim.-Waves (GSMM)*, May 2012, pp. 351–354.
[23] S. Cheng, E. Ojefors, P. Hallbjorner, and A. Rydberg, "Compact reflective microstrip phase shifter for traveling wave antenna applications," *IEEE Microw. Wireless Compon. Lett.*, vol. 16, no. 7, pp. 431–433, Jul. 2006.
[24] C.-L. Hsu, "Dual-band branch line coupler with large power division ratios," in *Proc. Asia–Pacific Microw. Conf. (APMC)*, Dec. 2009, pp. 2088–2091.
[25] T. Kawai, H. Taniguchi, I. Ohta, and A. Enokihara, "Broadband branch-line coupler with arbitrary power split ratio utilizing microstrip series stubs," in *Proc. 40th Eur. Microw. Conf. (EUMC)*, Sep. 2010, pp. 1170–1173.
[26] Y. Wu, S. Y. Zheng, S.-W. Leung, Y. Liu, and Q. Xue, "An analytical design method for a novel dual-band unequal coupler with four arbitrary terminated resistances," *IEEE Trans. Ind. Electron.*, vol. 61, no. 10, pp. 5509–5516, Oct. 2014.
[27] E. D. Lin, Y.-H. Pang, and H.-C. Huang, "Ring-resonator branch-line coupler with unequal power division," in *Proc. Asia–Pacific Microw. Conf. (APMC)*, Nov. 2014, pp. 699–701.
[28] Y.-M. Cai, K. Li, Y.-Z. Yin, and W. Hu, "Broadband circularly polarized printed antenna with branched microstrip feed," *IEEE Antennas Wireless Propag. Lett.*, vol. 13, pp. 674–677, 2014.
[29] Y. P. Zhang and J. J. Wang, "Theory and analysis of differentially-driven microstrip antennas," *IEEE Trans. Antennas Propag.*, vol. 54, no. 4, pp. 1092–1099, Apr. 2006.
[30] Y. P. Zhang, "Design and experiment on differentially-driven microstrip antennas," *IEEE Trans. Antennas Propag.*, vol. 55, no. 10, pp. 2701–2708, Oct. 2007.
[31] W. R. Eisenstadt, B. Stengel, and B. M. Thompson, *Microwave Differential Circuit Design Using Mixed-mode S-Parameters*. Boston, MA, USA: Artech House, 2006.
[32] D. M. Pozar, *Microwave Engineering*, 3rd ed. New York, NY, USA: Wiley, 2005.

Lin Li received the B.S. degree in electrical engineering and the M.S. degree in electronic science and technology from Zhejiang University, Hangzhou, China, in 1999 and 2005, respectively, and the Ph.D. degree in electromagnetic field and microwave technology from Shanghai Jiaotong University, Shanghai, China, in 2009.

Since 2010, he has been an Associate Professor with the College of Information, Zhejiang Sci-Tech University, Hangzhou, China. He is currently a Post-Doctoral Fellow with Shanghai Jiao Tong University. His current research interests include microwave integrated circuits and antenna technologies.

Jun-Fa Mao (M'92–SM'98–F'12) was born in 1965. He received the B.S. degree in radiation physics from the University of Science and Technology of National Defense, Changsha, China, in 1985, the M.S. degree in experimental nuclear physics from the Shanghai Institute of Nuclear Research, Chinese Academy of Sciences, China, in 1988, and the Ph.D. degree in electronic engineering from Shanghai Jiao Tong University, Shanghai, China, in 1992.

From 1994 to 1995, he was a Visiting Scholar with the Chinese University of Hong Kong, Hong Kong. From 1995 to 1996, he was a Post-Doctoral Researcher with the University of California at Berkeley, Berkeley, CA, USA. Since 1992, he has been a faculty member with Shanghai Jiao Tong University, where he is currently a Chair Professor and the Vice President. He is a member of the Chinese Academy of Science. He has authored or co-authored over 400 papers (including over 120 IEEE journal papers). His current research interests include interconnect and package problem of integrated circuits and systems, and analysis and design of microwave components and circuits.

Dr. Mao was a member of the 2012–2014 IEEE Microwave Theory and Techniques Society Fellow Evaluation Committee and the 2015 IEEE Fellow Committee. He is a Fellow of the CIE. He was the recipient of the National Natural Science Award of China in 2004, the National Technology Invention Award of China in 2008, the National Science and Technology Advancement Award of China in 2012, and six Best Paper Awards of international conferences. He is a Chief Scientist of the National Basic Research Program (973 Program) of China, a Project Leader of the Natural Science Foundation of China for Creative Research Groups, a Cheung Kong Scholar of the Ministry of Education, China, the Director of the Microwave Society of China Institute of Electronics, and the Chair of the IEEE MTT-S Shanghai Chapter from 2009 to 2018. He was the founder and the Chair of the IEEE Shanghai Section from 2007 to 2009.

Lin-Sheng Wu (S'09–M'10–SM'15) was born in 1981. He received the B.S. degree in electronic and information engineering and the M.S. and Ph.D. degrees in electromagnetic fields and microwave technologies from Shanghai Jiao Tong University (SJTU), Shanghai, China, in 2003, 2006, and 2010, respectively.

From 2010 to 2012, he was a Post-Doctoral Fellow with SJTU, where he is currently an Associate Professor with the Key Laboratory of Ministry of Education of Design and Electromagnetic Compatibility of High-Speed Electronic Systems. In 2010 and from 2012 to 2013, he was a Research Fellow with the Department of Electrical and Computer Engineering, National University of Singapore, Singapore. He has authored or co-authored over 100 technical papers. His current research interests include novel techniques for microwave integration, passive components, and carbon nano-electromagnetics.

Dr. Wu was the recipient of the National Natural Science Fund for Outstanding Young Scholars of China in 2016. He is also a Reviewer for several international journals, including six IEEE TRANSACTIONS and LETTERS.